AD-753 385

GEOMETRICAL ACOUSTICS AT MICROWAVE
FREQUENCIES

B. A. Auld, et al

Stanford University

Prepared for:

Office of Naval Research

December 1972

GEOMETRICAL ACOUSTICS AT MICROWAVE FREQUENCIES
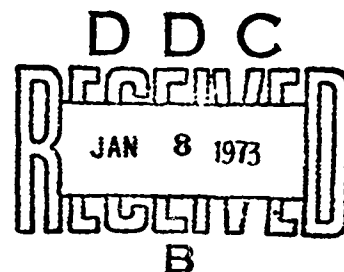
ANNUAL REPORT

1 November 1971-31 October 1972

for

Navy Office of Naval Research

Contract No. N00014-67-A-112-0001

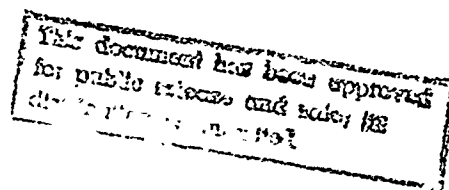M. L. Report No. 2123

December 1972

Microwave Laboratory
W. W. Hansen Laboratories of Physics
Stanford University
Stanford, California

GEOMETRICAL ACOUSTICS AT MICROWAVE FREQUENCIES

OBJECTIVE

The purpose of this investigation is to study focusing and deflection of microwave acoustic bulk wave and surface wave beams in inhomogeneous anisotropic solids and to evaluate potential device applications of these effects. Initially, the emphasis was on strictly geometrical effects and on inhomogeneities induced by means of magnetic and electric fields applied to ferromagnetic and semiconducting crystals. The investigation was later expanded to include diffraction effects and optically induced inhomogeneities, using mechanisms such as photoconductivity in piezoelectric media.

I. CONTROL OF ACOUSTIC SURFACE WAVES WITH PHOTOCONDUCTIVE FILMS

A. Introduction

In Reference 1, experiments were described in which an acoustic surface wave is reflected by an optically induced pattern of conductivity in a photo-conductive CdS film overlay on the substrate surface. The pattern (which is produced by imaging the shadow of an appropriate mask onto the CdS film) has the form of a grating of illuminated quarter-wavelength bars, with quarter-wavelength spacings. If the bar width and spacing is increased to one-half wavelength, the same interaction leads to scattering from a normally-incident longitudinal volume wave into a surface wave (Fig. 1). Volume-to-surface scattering of this kind has now been observed experimentally and is found to be in fairly good agreement with theoretical predictions.

B. Theory

A Born perturbation analysis of volume-to-surface scattering and surface-to-surface scattering has been developed by using the normal mode approach
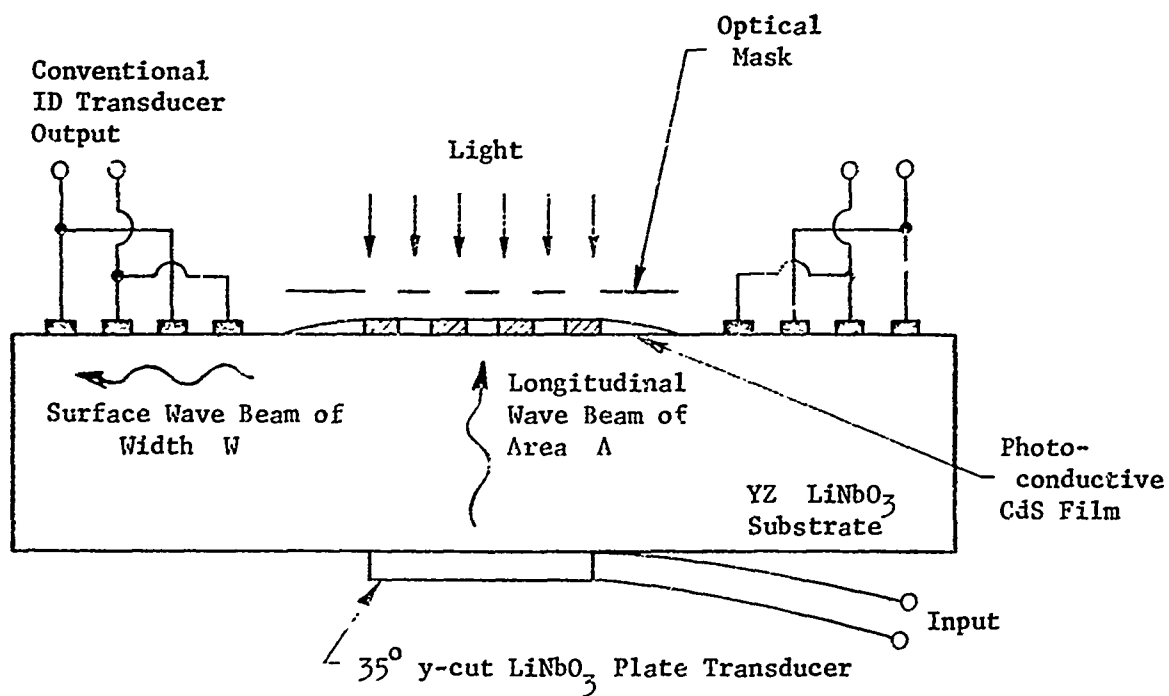
- 1 -

FIG. 1--Photoconductive scattering of a longitudinal volume
wave into a surface wave.

to surface wave analysis.[2,3] Only the lowest order term is retained in the perturbation calculation. The scattering calculation can therefore be carried out first for a single bar of the grating (Figs. 2 and 3) and then summed over the entire grating.

If the photoconductive effect is assumed to be isotropic, the permittivity of the illuminated regions in the CdS film is changed from $\underset{\approx}{\epsilon}^T$ to

$$\underset{\approx}{\epsilon}^{T'} = \underset{\approx}{\epsilon}^T + e\, K\, I(y,z)/i\omega \tag{1}$$

where e is a perturbation parameter and

$$K = \text{photoconductive constant}$$

$$I(y,z) = \text{optical illumination intensity}$$

The perturbed electric and acoustic fields are then expressed as

$$\underset{\sim}{E}' = \underset{\sim}{E}^{(0)} + e\underset{\approx}{E}^{(1)} + \ldots$$

$$\underset{\sim}{D}' = \underset{\sim}{D}^{(0)} + e\underset{\sim}{D}^{(1)} + \ldots$$

$$\underset{\approx}{T}' = \underset{\approx}{T}^{(0)} + e\underset{\approx}{T}^{(1)} + \ldots \tag{2}$$

$$\underset{\sim}{v}' = \underset{\sim}{v}^{(0)} + e\underset{\sim}{v}^{(1)} + \ldots$$

These fields must satisfy the divergence equation

$$\nabla \cdot \underset{\sim}{D}' = 0 . \tag{3}$$

with

$$\underset{\sim}{D}' = \underset{\approx}{\epsilon}^{T'} \cdot \underset{\sim}{E}' + \underset{\approx}{d} : \underset{\approx}{T}'$$

As in the derivation of Ingebrigtsen's perturbation formula, the assumption is made that the stress field is essentially unperturbed.[2] The first-order term in (3) is then

$$\nabla \cdot \underset{\approx}{\epsilon}^{T} \cdot \underset{\approx}{E}^{(1)} = \rho_{equiv} \tag{5}$$

where

$$\rho_{equiv} = \frac{K}{i\omega} \nabla \cdot 1 (y,z) \underset{\sim}{E}^{(0)} \tag{6}$$

is the equivalent source of the first-order field. One first evaluates ρ_{equiv} from the zero-order (or incident wave) field. The first-order (or scattered wave) field can then be obtained from the mode amplitude equation [2,3]

$$\left(\frac{\partial}{\partial z} - i\beta_R\right) a_{R-(z)} = f(z) , \tag{7}$$

where

$a_{R-(z)}$ = amplitude of the scattered surface wave traveling to the left in Figs. 2 and 3

$$f(z) = - N_R \int_{-H}^{0} \Phi_R^*(y) (i\omega \rho_{equiv}(y,z)) \, dy$$
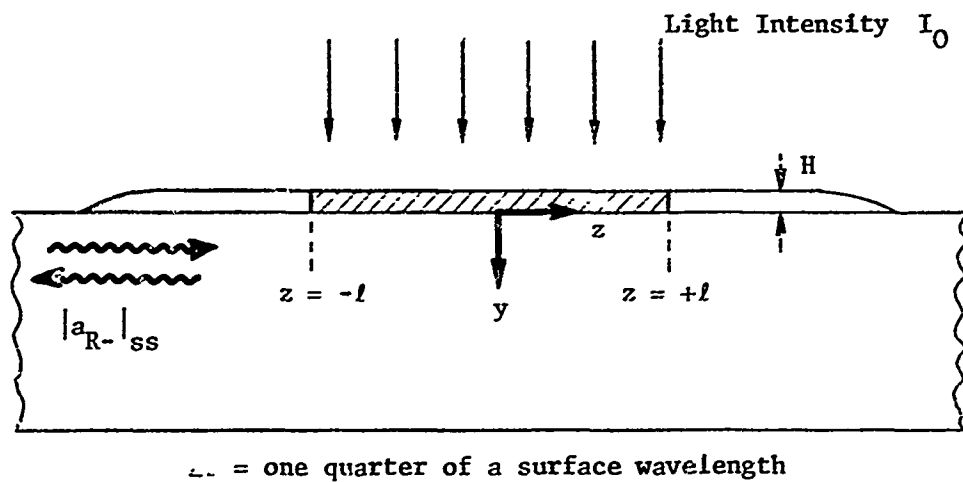
- 4 -

Light Intensity I_0

ℓ = one quarter of a surface wavelength

FIG. 2--Surface wave to surface wave scattering at a single
photoconductive bar.

Light Intensity I_0

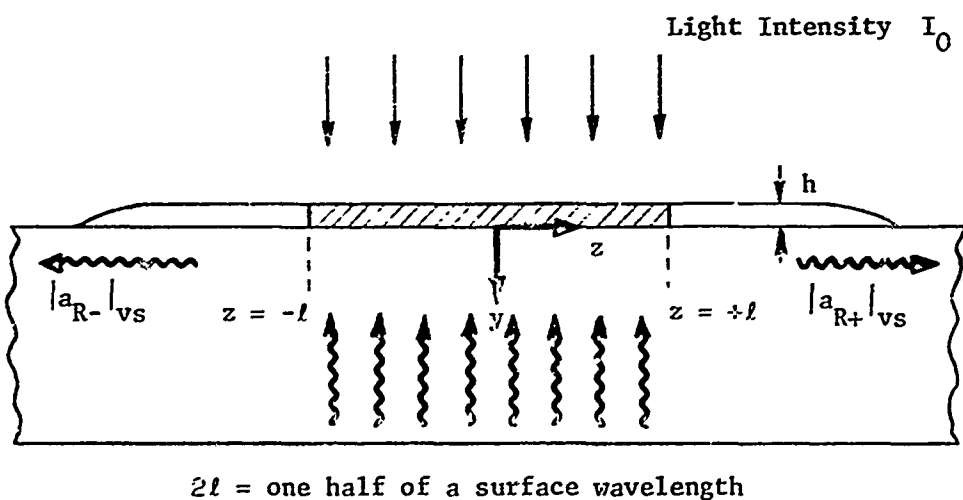2ℓ = one half of a surface wavelength

FIG. 3--Volume wave to surface wave scattering at a single
photoconductive bar.

- 5 -

$$\Phi_R(y) = \text{electrical potential field for a unit amplitude surface wave}$$

$$P_R = \text{power density/unit width for a unit amplitude surface wave}$$

A computer calculation of the surface wave fields in the CdS layer shows that Φ_R is constant to an accuracy of $\pm 10\%$ and can therefore be removed from the integral in $f(z)$.

From (6) and (7), the amplitude of the scattered surface wave is[2]

$$|a_{R_-}| = K \frac{\Phi_R^*}{4P_R} \int_{-\ell}^{+\ell} \int_{-H}^{0} \left\{ \frac{\partial}{\partial y} (IE_y^{(0)}) + \frac{\partial}{\partial z} (IE_z^{(0)}) \right\} e^{-i\beta_{Rz}} \, dy \, dz \qquad (8)$$

where β_R is the surface wave propagation factor. The illumination intensity I is independent of z within the bar ($-\ell$ to $+\ell$ in Figs. 2 and 3) and varies exponentially with y. That is

$$I = I_o e^{-2\alpha_0(y+H)}, \qquad (9)$$

where $2\alpha_0$ is the optical absorption factor in the CdS. For volume-to-surface scattering, the zero order field is independent of z and the second term in (8) is zero. In the surface-to-surface case the second term is not identically zero but it can be shown to be of negligible importance compared with the first. The scattered wave amplitude is therefore

- 6 -

$$|a_{R-}| = KI_0 \frac{\Phi_R^*}{4P_R} \int_{-\ell}^{+\ell} \left(e^{-2\alpha_0 H} E_y^{(0)}(0) - E_y^{(0)}(-H) \right) e^{-i\beta_R z} dz \qquad (10)$$

To evaluate (10), one must consider the volume-to-surface and surface-to-surface problems separately. Details of the calculation will b~ given in a journal publication now in preparation. For the geometry shown in Fig. 1, with $n = 1$ μm and a frequency of 102.5 MHz the scattered wave amplitude for surface-to-surface scattering is

$$|a_{R-}|_{ss} = 5.75 \times 10^4 \frac{KI_0}{\beta_R} \frac{\Phi_R^*}{4P_R} p_s^{1/2} \qquad (11)$$

and for the (longitudinal) volume-to-surface scattering it is

$$|a_{R-}|_{vs} = 7 \times 10^{10} \frac{KI_0}{\beta_R} \frac{\Phi_R^*}{4P_R} p_v^{1/2} \, , \qquad (12)$$

with

p_s = power density/unit width for the incident surface wave

p_v = power density/unit area for the incident volume wave

From (11) and (12) the ratio of the scattered powers is

$$\frac{(p_{out})_{vs}}{(p_{out})_{ss}} = 1.44 \times 10^{-6} \frac{(I_0)_{vs}}{(I_0)_{ss}} \frac{p_v}{p_s}$$

- 7 -

This is for a single grating bar in each case. Summing the scattered wave amplitudes over the N bars in the grating gives a scattered power proportional to N^2. One then has

$$\frac{\left(P_{out}/P_{in}\right)_{vs}}{\left(P_{out}/P_{in}\right)_{ss}} = 1.44 \times 10^{-6} \frac{w}{A} \frac{\left(N^2 I_0\right)_{vs}}{\left(N^2 I_0\right)_{ss}} \quad , \tag{13}$$

where

$$P_v = \left(P_{in}\right)_{vs}/A$$

$$P_s = \left(P_{in}\right)_{ss}/w$$

from Fig. 1.

C. Experimental Results

Experiments were performed at 102.5 MHz , using a 16 bar photo-conductive grating for volume-to-surface scattering and a 20 bar grating for surface-to-surface scattering. Optical illumination was provided by the pulsed argon laser described in Reference 1. The width w of the surface wave beam and the area A of the longitudinal wave beam are

- 8 -

$$w = 1.45 \times 10^{-3} \, m$$

$$A = 1.265 \times 10^{-6} \, m^2$$

If the optical illumination intensity is the same for both volume-to-surface and surface-to-surface scattering, (13) predicts that the volume-to-surface scattering efficiency is 29.3 dB smaller than the surface-to-surface scattering. Experimentally observed results for several different systems were 33 dB , 31 dB , 38 dB , and 27 dB . It should be noted that the adjustment of the optical mask in order to obtain optimum scattering is quite critical, and there is no guarantee that the volume-to-surface and surface-to-surface scattering losses were measured under exactly the same conditions.

The experiments were usually performed by exciting a surface wave in Fig. 1 and detecting the scattering longitudinal volume wave. Spurious signals presented the major obstacle to getting a clear picture of the scattering. Echo patterns, resulting from excitation of the volume transducer by (a) direct electromagnetic radiation from the input interdigital transducer (b) electromagnetic radiation from the surface wave pickup transducer, and (c) possible acoustic reflections from the leading or trailing edges of the CdS film, all served to hide the scattered bulk wave. Eventually, careful shielding and grounding solved most of these problems. Fig. 4,

shows a sample of the volume wave transducer output with and without the optical grating pattern applied to the CdS.

The remaining problem is one of absolute scattering losses. Typically, in our experiments, we had total transducer losses averaging about 20 dB . Total insertion loss from input to output varied from 74 dB to 84 dB , and the absolute scattering loss therefore varies from 54 dB to 64 dB . It should be noted however that the surface-to-surface scattering ranged from 10 to 25 dB larger than the best value reported in Reference 1. The photoconductive quality of the CdS film is a critical factor and probably accounts for this difference in the observed surface-to-surface scattering. With a 5 dB surface-to-surface scattering loss, as given in Reference 1, one should expect a volume-to-surface scattering loss of 33 dB for a 20 bar grating. Theoretically, the scattering efficiency should vary as the square of N , the number of bars in the grating. It is to be expected that this relationship will be modified by attenuation due to the CdS conductivity and to multiple reflections, which have been ignored in the calculation. Surface-to-surface scattering measurements have shown that the scattering varies nearly with N rather than as N^2 . One should, therefore, still be able to reduce the scattering loss by increasing N .
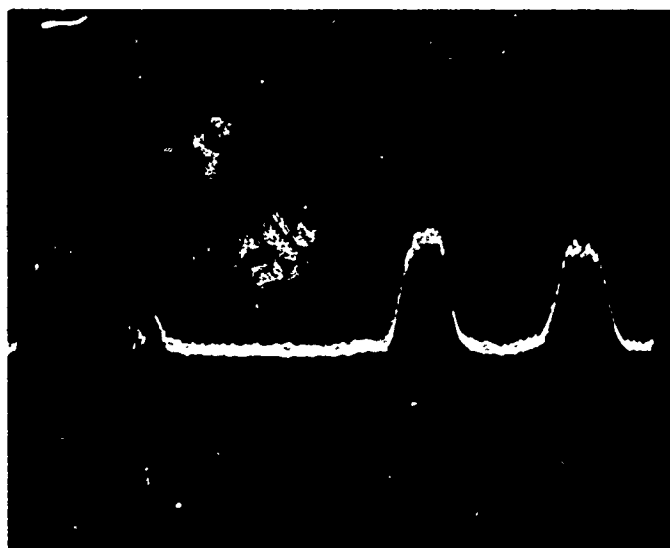
II. FRESNEL ZONE FOCUSING AND SCANNING OF VOLUME ACOUSTIC WAVES

A. Introduction

The purpose of this study is to investigate the focusing and scanning
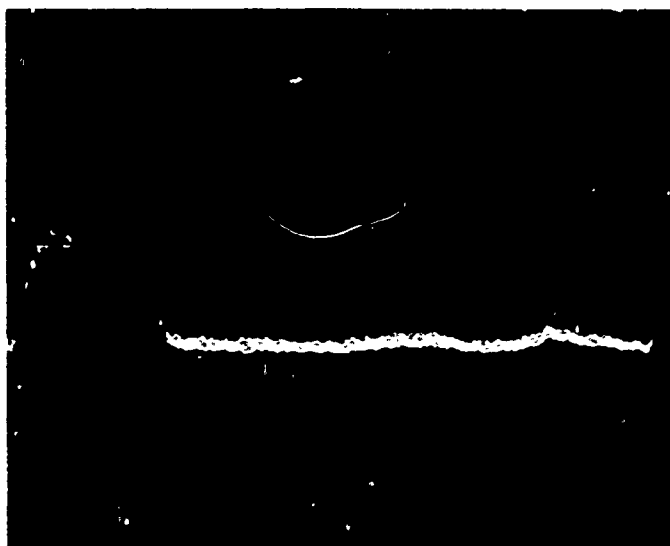
(a)

(b)

FIG. 4--Transmission from input to output transducer in Fig. 1.
(a) Laser off; (b) Laser on.

of acoustic beams using acoustic Fresnel zone plates with both fixed and photoconductive transducers. Some of the results have been described in the previous Annual Report (October 1971).

B. Calculated behavior

The concept of a zone plate was described in the previous report. For a monochromatic plane wave incident on the aperture plane of Fig. 5, Huygens wavelet construction at the aperture plane indicates that radiation of all phases reaches the point P . Blocking all but in-phase radiation should increase intensity over the uniform illumination case. From Fig. 5 , if the regions between r_2 and r_1 , r_4 and r_3 etc. are made nonradiating, and if $R_n = R_0 + \frac{n\lambda}{2}$, all energy at P will be in phase. From the diagram

$$R_0^2 + r_n^2 = R_n^2 \quad .$$

For cases where $R_0 \gg n\lambda$, this reduces to

$$r_n^2 = n\lambda R_0 = n r_1^2 \tag{1}$$

where it is seen directly that the focal length, R_0 is a function of frequency

The behavior of a given zone plate constructed in accordance with (1) may be calculated using the Rayleigh-Sommerfeld diffraction integral

$$\frac{U(x_0,z)}{U_0} = \frac{k_0}{j2\pi z} \int_0^{2\pi}\int_\rho \rho \exp\left[j\frac{k_0}{2z} \left(x_0^2 + \rho^2 - 2\rho x_0 \cos\theta \right) \right] d\rho\, d\theta \tag{2}$$
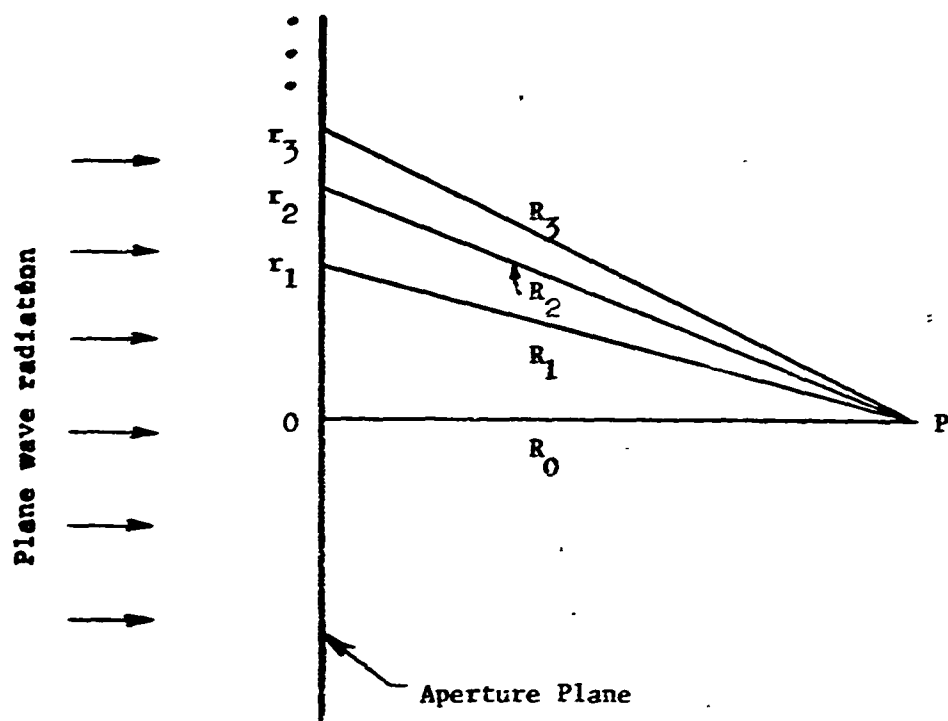
FIG. 5--Fresnel zone plate construction.

where $U(x_0,z)/U_0$ is the normalized complex field amplitude. Most of the experiments performed involve ten zone lenses.

The intensity gain over isotropic at the principle focus is 400, corresponding to the rule

$$\left[\frac{U(x_0,y_0,z)}{U_0}\right]^2 = \left[\frac{U(0,0,R_0)}{U_0}\right]^2 = 4N^2$$

where N is the number of zones.

Matters become more complicated when the acoustic medium is anisotropic, k is no longer a constant but rather

$$k(\theta) = k_0 (1 - b\theta^2)$$

for longitudinal acoustic waves propagating close to the three- , four- , and six-fold pure modes axes.[*] Equation (2) must then be corrected to

$$\frac{U(x_0,z)}{U_0} = \frac{k_0}{j2\pi z(1-2b)} \int\!\!\int_0^{2\pi} \rho \, \exp\left[j\frac{k_0}{2z(1-2b)}\left(x_0^2 + \rho^2 - 2\rho x_0 \cos\theta\right)\right] d\rho d\theta \tag{3}$$

from which it is seen that the focal length has increased by a factor $1/(1-2b)$.

---

[*]Here, b is called the anisotropy factor.

C. Experiment

An experiment is being performed in which the Fresnel zone plate transducer described in the Annual Report of November 1971 is used to focus the acoustic beam onto a thin water layer on the end of the sapphire crystal. In this case the zone plate is etched into the counter electrode of the nonphotoconductive ZnO transducer deposited on the sapphire crystal and an Au-SiO impedance matching transformer is deposited on the other end in order to match into the water. The cross section of the acoustic beam is visualized by placing small plastic balls (1-7 μm in diameter) in the liquid and observing the displacements with 50 X optical magnification.[4] Fig. 6 shows the focal plane intensity distribution as seen by using 1.1 μ balls in a thin layer of water, sandwiched between the crystal and a transparent lucite plate. The central spot is approximately 20 μm in diameter, as expected from the theory. Fig. 7 shows the intense streaming pattern that results when a drop of water containing 3 - 7 μ balls is simply placed on the crystal.

III. SUMMARY AND PROJECTION

Scattering of a surface acoustic wave into a volume wave by a photoconductive grating has been observed experimentally, the results being in fairly good agreement with theoretical predictions. A publication is now being prepared.

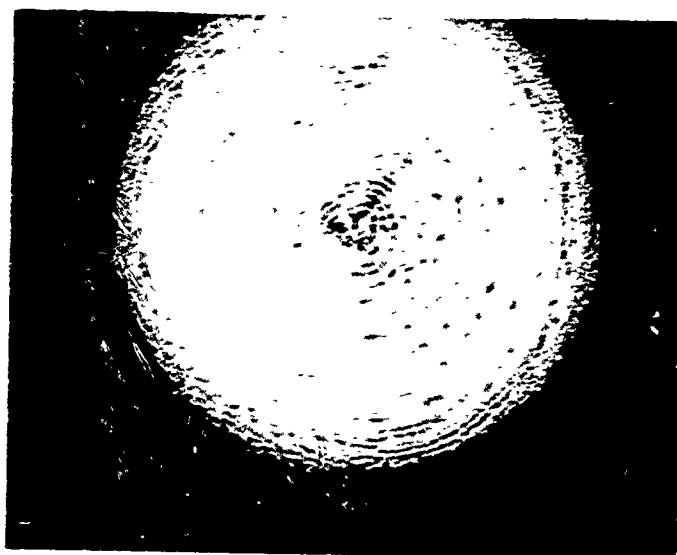Preliminary experimental observations have been made of the focal

FIG. 6--Focal plane intensity distribution seen by using 1.1 . balls in
a thin layer of water.

FIG. 7--Streaming pattern produced by the focused beam in a drop of
water containing 4 - 7 balls.

plane intensity distribution produced by an etched Fresnel zone plate transducer. More complete measurements are planned for this system, after which similar experiments will be carried out for the case of a photoconductive zone plate transducer. In the latter case, scanning of the focused beam is possible and the ultimate goal is to use this arrangement for scanned acoustic imaging.

References

1. B. A. Auld, D. A. Wilson, D. K. Winslow and E. Young, "Control of Acoustic Surface Waves with Photoconductive CdS Films," Applied Physics Letters 18, 339-341 (1971).

2. B. A. Auld, "Surface Wave Theory," pp. 1-15, Invited Proceedings 1970 Ultrasonics Symposium, IEEE Catalogue Number 70C69SU, (1971)

3. B. A. Auld and G. S. Kino, "Normal Mode Theory for Acoustic Waves and its Application to the Interdigital Transducer," IEEE Trans ED-18, pp. 898-908, (1971).

4. J. A. Cunningham and C. F. Quate, "Direct Visualization of Ultrasonic Interference in Solids," 4th Annual Symposium on Acoustical Holography, April 1972, Santa Barbara.

PERSONNEL

E.A. Auld,   Principle Investigator

S. Farnow   Research Assistant

Major Items of Equipment Purchased or Constructed:

   None

Trips, Meetings and Special Conferences:

   None

Publications:

   None